ACS Biomaterials SCIENCE & ENGINEERING

pubs.acs.org/journal/abseba

Article

Impedimetric Detection of Calreticulin by a Disposable Immunosensor Modified with a Single-Walled Carbon Nanotube-Conducting Polymer Nanocomposite

Elif Burcu Aydın,* Muhammet Aydın, and Mustafa Kemal Sezgintürk

Cite This: *ACS Biomater. Sci. Eng.* 2022, 8, 3773−3784

Read Online

ACCESS | Metrics & More | Article Recommendations | Supporting Information

ABSTRACT: A label-free impedimetric immunosensing system was constructed for ultrasensitive determination of the calreticulin (CALR) biological marker in human serum samples utilizing an electrochemical impedance spectroscopy analysis technique for the first time. The new biosensor fabrication procedure consisted of electrodeposition of single-walled carbon nanotubes (SWCNTs) incorporating polymerization of an oxiran-2-yl methyl 3-(1H-pyrrol-1-yl) propanoate monomer (*Pepx*) onto a low-cost and disposable indium tin oxide (ITO) electrode. The *SWCNTs-PPepx* nanocomposite layer was prepared onto the ITO after the one-step fabrication procedure. The fabrication procedure of the immunosensor and the characteristic biomolecular interactions between the anti-CALR and CALR were characterized by electrochemical analysis and morphological monitoring techniques. Under optimum conditions, the proposed biosensor was responsive to CALR concentrations over the detection ranges of 0.015−60 pg/mL linearly, and it had a very low detection limit (4.6 fg/mL) and a favorable sensitivity (0.43 kΩ pg^{-1} mL cm^{-2}). The reliability of the biosensor system in clinical analysis was investigated by successful quantification of CALR levels in human serum. Moreover, the repeatability and reproducibility results of the biosensor were evaluated by using Dixon, Grubbs, *T*-test, and *F*-tests. Consequently, the proposed biosensor was a promising method for scientific, rapid, and successful analysis of CALR in human serum samples.

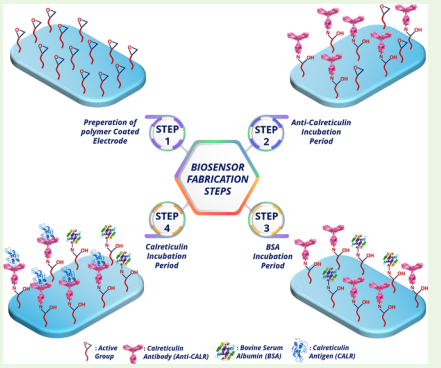

KEYWORDS: *breast cancer, calreticulin, disposable immunosensor, impedimetric detection*

1. INTRODUCTION

Breast cancer is a serious health problem for females. The World Health Organization reported that 2.3 million woman were diagnosed with breast cancer and 685 deaths globally in 2020. Early diagnosis of cancer disease and efficient treatment can significantly reduce the breast cancer mortality and increase the survival rates.[1,2] The cancer diagnosis techniques contain clinical and physical investigations, histopathology, mammography, and ultrasound magnetic resonance imaging, but they are not adequate to determine the breast cancer at early stages.[3,4] Although breast cancer detection with mammography is usually achieved with high efficiency, it only allows the visualization of the tumor and cannot predict its biological behaviors. Current studies are focused on the analysis of cancer markers in biological fluids for early diagnosis of breast cancer. Cancer markers are biological indicators which can illustrate the variations in the structure or function of the human body. Therefore, biomarkers play a significant role in illness diagnosis, choice of the treatment program, and assessment of prognosis.[1,5,6]

Calreticulin (CALR) is a calcium-binding chaperon protein (46 kDa) present in the endoplasmic reticulum lumen.[7,8] CALR has two primary roles, being a molecular chaperone and a regulator of intracellular calcium ion homeostasis.[9] CALR controls the appropriate folding of produced proteins and membrane-bound surface biomolecules that are significant in the cell communication with its external surroundings. The calcium ion is the secondary reporter element in several intracellular signaling pathways, and therefore, CALR is an important part of cell signaling.[7,10] CALR is a very promising breast cancer biomarker about invasion and metastasis, and it is upregulated significantly in N0, N1, and N2 stages of breast cancer.[11,12] Ni et al. reported that the CALR concentration in human serum was 3.726 ± 0.627 (n = 35) ng/mL.[13] In clinical analysis, enzyme-linked immunoassay (ELISA) is usually utilized for CALR detection in human body fluids. This technique is based on colorimetric reading and gives reproducible, accurate, and reliable results. This advantage makes it a suitable tool for clinical diagnosis.[14] However, this technique has some shortcomings including a long and

Received: April 28, 2022
Accepted: July 20, 2022
Published: August 3, 2022

exhausting assay procedure, demand for skilled professionals, excess chemical requirement, short shelf life of the labeled antibody, a narrow detection range, and high cost.[15−18] The detection limit of ELISA is less than the nanogram concentration level that is insufficient to obtain the threshold of protein markers, especially in the early step of diseases.[19,20] In addition, commercial ELISA is not suitable for reuse. In contrast to immunoassays, in immunosensors the same bioreceptor layer can be reused for many measurements after regeneration in basic solution (NaOH/NaCl) or glycine/HCl buffer solution for few minutes. These causes restrict their commercial usage in the medical field.[21] Immunosensors are interesting tools because of their simple utilization, suitable efficiency, possibility of portability, real time analysis, low cost, and excellent selectivity and sensitivity.[22−24] Because of their promising properties, they have been usually utilized in diverse fields including clinical analysis, food control, environmental monitoring, and pharmaceutical and biological-warfare agents' analyses.[25−27]

Electrochemical polymerization is an efficient technique for sensing platform modification with targeted characteristics, high stability, and excellent homogeneity. Because of this, this technique is frequently utilized for sensing surface modification.[28] Electrochemical impedance spectroscopy (EIS) is a versatile, nondestructive technique to follow the characterization of the surface-functionalized electrode.[29,30] This technique characterizes the electron transport as well as the impedance between the electroactive species and electrode surface.[31] Impedimetric immunosensors that integrate immunosensors with the EIS technique have been progressively used for label-free determination of food contaminants, cancer and cardiac biomarkers, and environmental analysis.[32] The binding of biorecognition molecules on the working electrode is also important to improve the electrochemical feature and the use of the biosensor. The covalent immobilization of the biorecognition elements provides a highly efficient electrode surface.[33]

Nanomaterials like nanoparticles, nanotubes, and nanohybrid materials are utilized in the attractive research field because of their unique chemical and physical properties such as a large surface area, high conductivity, and good biocompatibility.[34−36] Carbon nanotubes (CNTs), classified as multiwalled carbon nanotubes (MWCNTs) and single-walled carbon nanotubes (SWCNTs), have gained a lot of interest since being discovered by Iijima in 1991. The excellent structural, electrical, mechanical, and thermal features of CNTs provide development of new and sensitive sensing tools including electrochemical biosensors. They are proper materials for the modification of working electrodes because of their high electrical conductivity for electron transfer reactions and high stability. Accordingly, development of effective electrochemical biosensors based on CNT-modified working electrodes is a very promising tool for the analysis of various target analytes.[37] The production of polymer/CNT composites is an effective way for biosensing applications, because combining CNTs with a polymer matrix advances mechanical and electrical features of the interface material. In addition, the incorporation of a CNT material into a polymer matrix effects the charge transfer behavior and also electrochemical features of the electrode surface that may be advantageous for biosensing applications.[38,39] Conjugated polymers as immobilization matrices provide improvements in biosensor design.[40−42] Among the conjugated polymers, polypyrrole is usually employed in biosensor construction because of its suitable electrical conductivity, good stability, ease of preparation, and biocompatibility. The biocompatibility property of polypyrrole makes it a proper immobilization matrix material for binding of biorecognition molecules. Furthermore, polypyrrole can be synthesized with electrochemical polymerization on the electrode surface.[43,44] Polypyrrole, a particular conducting polymer with a high application potential, is a quite suitable candidate for the synthesis of nanotube composites and appropriate for being an immobilization matrix material.[45] In a previous study, a polyaniline-SWCNT nanocomposite was synthesized on the working electrode, and the prepared electrode was utilized for detection of triglyceride.[38] Thus far, no attempt has been documented to fabricate an immunosensor based on the *SWCNTs-PPepx* nanocomposite for the determination of CALR in human serum.

This work described a novel strategy for the construction of an *SWCNTs-PPepx* nanocomposite layer which was fabricated by simultaneous electrodeposition of SWCNTs incorporating polymerization of the *Pepx* monomer onto disposable ITO electrodes. So far, SWCNTs have been deposited in the presence of a monomer without bearing active groups during the electropolymerization process. In this study, we prepared an *SWCNTs-PPepx* nanocomposite layer on the ITO working electrode by a one-step electrodeposition technique. The thickness of the nanocomposite layer can be readily controlled with the electrodeposition method, an evident superiority over the drop-casting technique. In addition, by using this technique, electrode surfaces homologous to each other were obtained. The *SWCNTs-PPepx* nanocomposite with considerable conductivity provided a biocompatible immobilization support for anti-CALR attachment via covalent binding between epoxy ends of *PPepx* and amino ends of anti-CALR. This immobilization procedure did not require crosslinking reactants. In this study, we prepared an SWCNTs-PPepx nanocomposite layer on the ITO working electrode by a one-step electrodeposition technique. The thickness of the nanocomposite layer can be readily controlled with the electrodeposition method, an evident superiority over the drop-casting technique. In addition, by using this technique, we can obtain more homogeneous electrode surfaces.

These impedimetric immunosensor fabrication stages were followed by performing EIS and cyclic voltammetry (CV) in the presence of $[Fe(CN)_6]^{3-/4-}$ as a redox probe. EIS results illustrated that a label-free and ultrasensitive analysis tool was developed for investigation of anti-CALR-CALR binding. Furthermore, the surface morphology of the modified working electrode surface was characterized by scanning electron microscopy (SEM) and atomic force microscopy (AFM). The suggested immunosensor displayed a low detection limit, good repeatability, long shelf life, and suitable performance in CALR determination in human sera.

2. EXPERIMENTAL SECTION

Materials and reagents used during the biosensor development are described in the Supporting Information.

2.1. Synthesis of Monomer Pepx. In brief, the monomer (*Pepx*) was synthesized by two reaction steps (hydrolysis and esterification) according to the literature report with minor modifications.[46−48] The first reaction step was the alkaline hydrolysis reaction of 1-pyrrolepropionitrile, and *N*-pyrrolylpropanoic acid (P-COOH) was produced. The second reaction step was the esterification reaction of *N*-pyrrolylpropanoic acid and glycidol, and the *Pepx* compound was

https://doi.org/10.1021/acsbiomaterials.2c00499
ACS Biomater. Sci. Eng. 2022, 8, 3773−3784

Scheme 1. Schematic Diagram of the Construction Process of the Label-Free Immunosensor for CALR with the *SWCNTs-PPepx* Nanocomposite-Coated Disposable Electrode

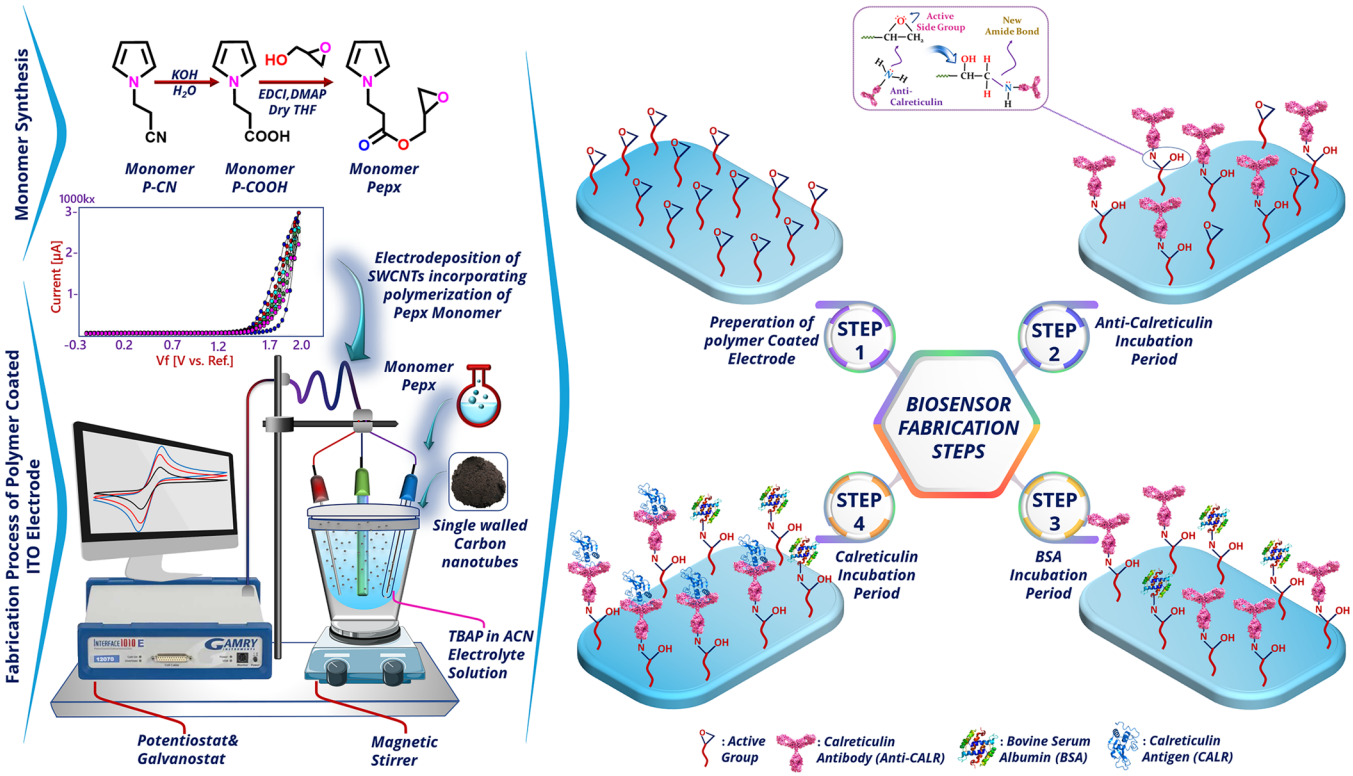

produced. The production pathway of the *Pepx* monomer is shown in Scheme 1.

Monomer (P-COOH) was a white solid: (Yield: %85, 4.87 g). FTIR cm^{-1}: 3500−3100; 2941; 2880; 1694; 1600−1450; 1216; 930; 786, 724; 647; 613. Raman (λ_{laser} = 780 nm): 1720 (C═O); 1600; 1460; 1320; 1120; 1046; 932; 764; 695. ^{1}H-NMR ($CDCl_3$, ppm): 11.6 (1H); 2.87 (1H); 4.24 (2H); 6.72 (2H) and 6.20 (2H).

Monomer (*Pepx*) was a pale-yellow liquid: (Yield: %55, 0.175 g). FTIR cm^{-1}: 2931−2880; 1730; 1502; 1450; 1157; 1090; 932; 908; 852; 785; 720; 659. Raman (λ_{laser} = 780 nm): 1738 (C═O); 1501; 1388; 1285; 1259; 1091; 1060; 976; 907;875; 852; 763; 702; 660; 616. ^{1}H-NMR ($CDCl_3$, ppm): 6.14 (2H); 6.67 (2H); 4.14 (2H); 2.83 (2H); 4.45 and 3.24 (2H); 3.94 (1H); 2.61 and 2.72 (2H).

2.2. Sensing Surface Preparation. Prior to modification, ITO sheets (20 mm × 5 mm) were successively ultrasonicated in acetone, soap solution (10% NaOH, 90% ethanol), and ultrapure water followed by rinsing thoroughly with ultrapure water. To prepare nanocomposite-coated electrodes, an electrolyte solution (100 mM tetrabutylammonium chloride (TBAPCl) in acetonitrile (ACN)) containing 20 μL of *Pepx* monomer (20 mg/mL) and 20 mg of SWCNTs was prepared. Then, the clean ITO surface was placed in a conventional three-electrode system and, electropolymerization of the *Pepx* monomer and electrodeposition of SWCNTs were performed by CV with the potential from −0.2 to 2 V for four cycles with a scan rate of 50 mV/s. During the electropolymerization and electrodeposition processes, the *Pepx* monomer-SWCNT solution (TBAPCl) was stirred with magnetic stirring. After electropolymerization and electrodeposition processes, the nanocomposite-coated electrode was washed with ACN and ultrapure water. Following the electrode preparation process, the prepared electrodes were immersed in anti-CALR solution for 45 min. Afterward, these electrodes were washed with ultrapure water and introduced to BSA solution (0.5%) to block free ends of the polymer layer. After 1 h, these electrodes were washed with ultrapure water, and different concentrations of CALR antigen were applied on the working electrode surfaces. After each binding stage, the prepared electrode was characterized by EIS and CV measurements.

2.3. Electrochemical Measurement Conditions. EIS analyses were performed in 5 mM $[Fe(CN)_6]^{3-/4-}$ solution including 1 M KCl and ITO electrodes connected to a Gamry Potentiostat 1000 which was utilized for electrochemical analyses. EIS spectra were recorded at an alternative current voltage of 5 mV, with a direct current voltage of 0 V in the frequency range from 50 kH to 0.5 Hz. CV measurements were performed in the potential range of −0.5−1 V with a scan rate of 0.1 V/s. Single-frequency impedance (SFI) measurements were performed at a single frequency that was determined by the aid of the Bode plot. The SFI parameters were 13 Hz monitor frequency, 0.01 V alternative current voltage, and 0 V direct current voltage.

2.4. Selectivity Study. The selectivity study was performed by analysis of PBS solutions containing target CALR (2.5 pg/mL), neuron-specific enolase (NSE) (250 pg/mL), interleukin 1α (IL-1α) (250 pg/mL), interleukin 1β (IL-1β) (250 pg/mL), tumor necrosis factor alpha (TNF-α) (250 pg/mL), and interleukin 6 (IL 6) (250 pg/mL) solutions. The ITO/*SWCNTs-PPepx nanocomposite*/anti-CALR/BSA immunoelectrodes were incubated in these solutions for 30 min, and the response of these bioelectrodes was recorded.

2.5. Analysis of Human Serum Samples. The suggested biosensor was employed for the measurement of CALR concentration in human serum samples. Before the analysis, these samples were diluted 1000 times with PBS, and then, the prepared ITO/*SWCNTs-PPepx nanocomposite*/anti-CALR/BSA electrodes were incubated in this solution for 30 min. After 30 min, the ITO/*SWCNTs-PPepx nanocomposite*/anti-CALR/BSA electrode was rinsed with ultrapure water, and electrochemical analyses were performed. Furthermore, the standard addition technique was studied to determine the reliability and performance of the suggested immunosensor. All human serum analyses were performed repeated twice.

3. RESULTS AND DISCUSSION

In this study, an immunosensor specific to CALR was fabricated in four steps. First, the nanocomposite layer was

https://doi.org/10.1021/acsbiomaterials.2c00499
ACS Biomater. Sci. Eng. 2022, 8, 3773−3784

successfully constructed by electrodeposition of SWCNTs incorporating polymerization of *Pepx* onto the ITO electrode (Stage 1). Then, specific antibodies related to CALR protein were immobilized onto the *SWCNTs-PPepx* nanocomposite-modified electrode surface (Stage 2). After that, BSA molecules bound on the ITO/*SWCNTs-PPepx nanocomposite*/anti-CALR surface to block remaining active sites (Stage 3). Finally, CALR antigens were attached onto the ITO surface, and the specific reaction was determined utilizing EIS (Stage 4). The whole immunosensor construction pathway is schematically displayed in Scheme 1.

3.1. Chemical Characteristics of Functionalized Electrode Surfaces. The FTIR spectra were taken at first and second stages of the surface modification procedure in order to prove the successful *SWCNT-PPepx* nanocomposite layer formation and anti-CALR antibody immobilization. Figure 1A,B includes the FTIR spectra of the *SWCNTs-PPepx* composite layer-casted ITO surface (A) and the subsequent modification with anti-CALR (B). The presence of carbonyl groups (C═O) in the polymer layer was evidenced by a strong absorption peak at 1738 cm^{-1}. The absorption peaks at 953 and 864 cm^{-1} came from epoxy groups of *PPepx*. The most evident absorption bands on the ITO surface after anti-CALR binding were at 1640 and 1560 cm^{-1}. These bands suggested the presence of amide groups from the protein ($-CONH_2-$). The spectrum of the anti-CALR bound surface provided significant insight into the presence of antibodies on the composite layer.

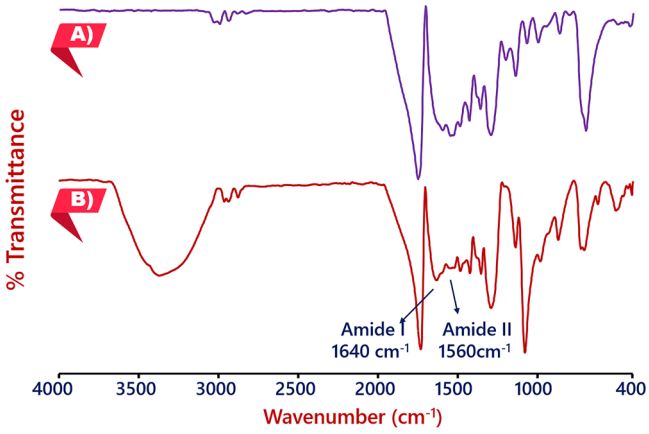

Figure 1. FTIR spectra of the *SWCNTs-PPepx* nanocomposite-coated ITO electrode (A) and anti-CALR attached electrode (B).

The energy-dispersive X-ray spectroscopy (EDX) study was also performed to investigate the electrode surface morphology. Figure SI-1A,B illustrates EDX spectra of SWCNTs and *SWCNTs-PPepx* composite layer-casted ITO surface, respectively. SWCNTs had oxygen (O), carbon (C), aluminum (Al), and sulfur (S) elements, and after nanocomposite coating, electrode included C, O, S, indium (In), tin (Sn), and nitrogen (N) elements. The peak of N originated from pyrrole rings of the *PPepx* polymer. Thus, these EDX images illustrated that the *SWCNTs-PPepx nanocomposite* was present on the ITO substrate surface.

3.2. Electrochemical Characteristics of Modified Electrode Surfaces. Scheme 1 demonstrates the modification pathway of the suggested immunosensor. Electropolymerization of the *Pepx* monomer was performed by using the CV technique with the potential range from −0.2 to 2 V. CVs obtained during the electrodeposition of SWCNTs incorporating polymerization of *Pepx* onto the ITO electrode are illustrated in Scheme 1. EIS and CV measurements were taken to follow the step-by-step modification process of the immunosensor. Figure 2A,B displays EIS and CV achieved at modified ITO electrodes in 5 mM $[Fe(CN)_6]^{3-/4-}$ including 1 M KCl. As seen in Figure 2A, a small Nyquist plot of the *SWCNTs-PPepx* nanocomposite layer was observed due to conductive properties of the *PPepx* polymer and SWCNTs. By fitting the obtained EIS data using the Randles equivalent circuit (inset Figure 2A), the electron transfer resistance was found as 1083 Ω. The Randles equivalent circuit was employed to define the measured EIS data. The used Randles equivalent circuit is shown in Figure 2A-inset, and this circuit has the ohmic resistance of redox probe solution (R_s), the Warburg impedance (W) arising from ion diffusion between the bulk electrolyte and the working electrode surface interface, the constant phase element (CPE), and the electron transfer resistance (R_{ct}).[49,50] The low R_{ct} indicated the fast electron transport kinetics of the redox couple at the ITO/*SWCNTs-PPepx nanocomposite* surface. As seen in Figure 2A, an increase in electron transfer resistance (2543 Ω) was seen in the presence of anti-CALR antibody. The anti-CALR proteins on the electrode surface formed a barrier, and this barrier made difficult the electron transfer. The blockage of epoxy ends by BSA on the electrode surface formed an insulative protein layer on the electrode surface, and it was more difficult for the redox probe. Thus, higher R_{ct} was measured (3785 Ω) due to

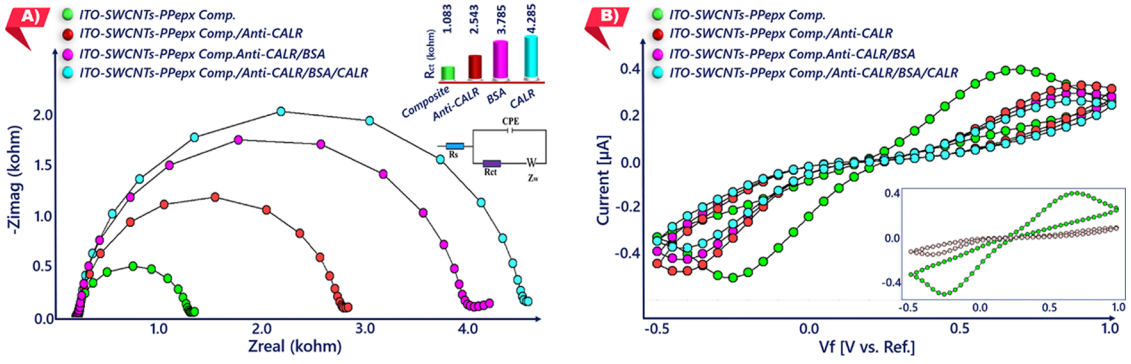

Figure 2. EIS spectra (A) and CV curves (B) of different stages of the electrode modification process in 5.0 mM of $[Fe(CN)_6]^{3-/4-}$ solution containing 1 M KCl.

https://doi.org/10.1021/acsbiomaterials.2c00499
ACS Biomater. Sci. Eng. 2022, 8, 3773−3784

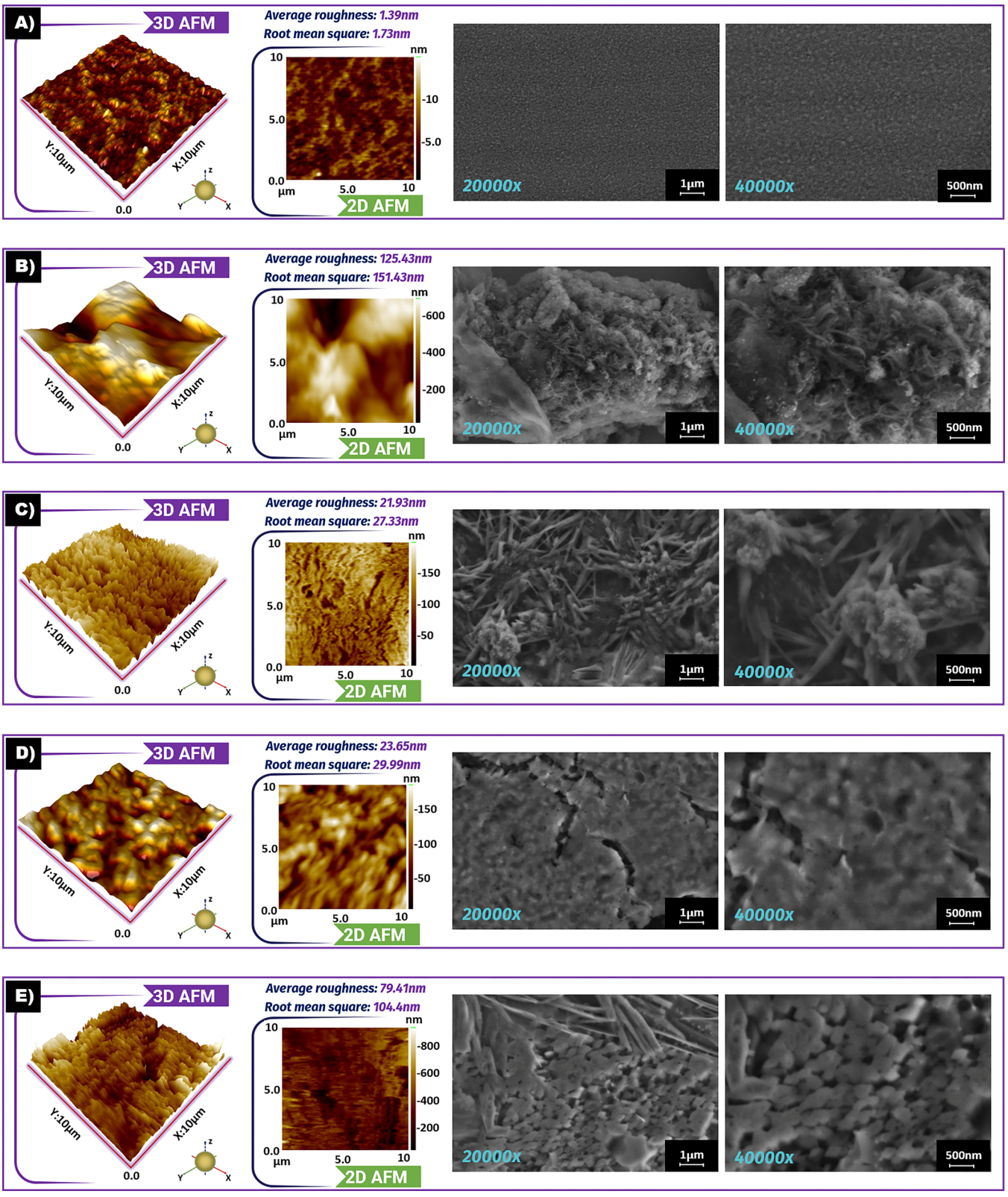

Figure 3. SEM and AFM images of the sequential modified layers on the ITO surface; (A) *Bare ITO*, (B) ITO/*SWCNTs-PPepx nanocomposite*, (C) ITO/*SWCNTs-PPepx nanocomposite*/anti-CALR, (D) ITO/*SWCNTs-PPepx nanocomposite*/anti-CALR/BSA, and (E) ITO/*SWCNTs-PPepx nanocomposite*/anti-CALR/BSA/CALR.

deceleration in electron transfer kinetics at the BSA protein-exposed immunoelectrode. At the last step of biosensor fabrication, the proteinous layer composed of anti-CALR and CALR antigen was formed due to specific antigen−antibody interactions, and this protein complex made electron transfer difficult for the redox reaction to happen, causing a large Nyquist plot (4285 Ω).

https://doi.org/10.1021/acsbiomaterials.2c00499
ACS Biomater. Sci. Eng. 2022, 8, 3773−3784

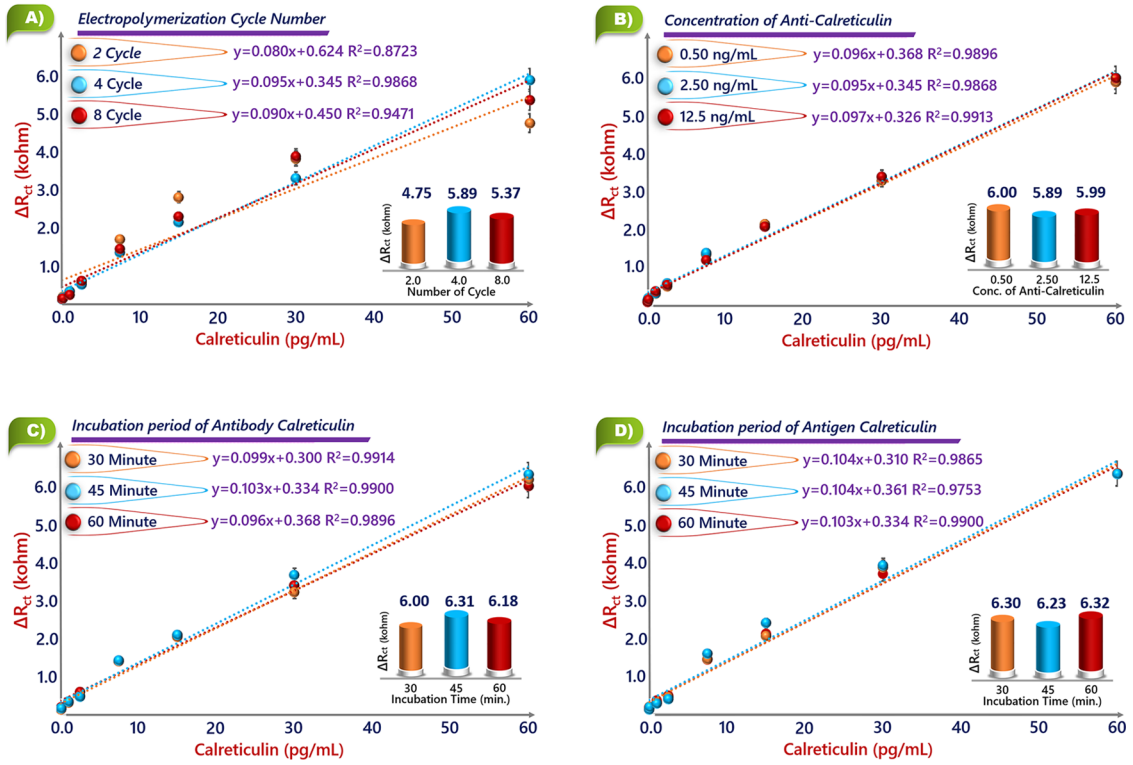

Figure 4. Condition optimization (A) *SWCNTs-PPepx* scan number; (B) anti-CALR concentration; (C) anti-CALR incubation duration; (D) CALR incubation duration.

Figure 2B depicts the cyclic voltammograms obtained during the biosensor fabrication steps. Figure 2B illustrates that a pair of redox peaks were observed at the *SWCNTs-PPepx* nanocomposite-modified ITO electrode. As seen in Figure 2B inset, with the nanocomposite layer coating on the ITO surface, the conductivity of the electrode surface increased and the peak currents were quite high after modification. After the binding process of anti-CALR on the nanocomposite-modified ITO electrode, a decrease in peak currents of the ferro-ferri redox probe was obtained because of formation of a protein barrier. The BSA layer formation on the free epoxy ends of the nanocomposite layer reduced the electron transfer rate, and decreases were observed in the peak currents of the redox probe. After anti-CALR and CALR complex formation, a barrier to the diffusion of ferro-ferri ions toward the ITO surface was observed, and this complex hindered the electron transfer process. Thus, decreases in peak currents were observed. The EIS and CV results showed the successful construction of the biosensor. The agreement of the EIS with CV results illustrated that the manufactured electrode was a perfect platform for CALR detection.

3.3. Morphological Characterization of Electrode Surfaces. SEM and AFM techniques are powerful tools for electrode surface morphology characterization of different electrode surfaces. The SEM and AFM images of the bare ITO electrode and *SWCNTs-PPepx* nanocomposite layer-modified electrodes are shown in Figure 3A,B, respectively. It can be seen that the two electrode surfaces had clearly different morphologies. The bare ITO had a homogeneous surface. The average roughness (R_a) of the bare electrode surface was as 1.39 nm, and the low R_a indicated the regular ITO surface. After the electropolymerization process, the SEM and AFM images of the *SWCNTs-PPepx* composite layer illustrated a three-dimensional (3D) network composed of a dense, compact, and homogeneous *PPepx* polymer layer and an SWCNT nanomaterial. The R_a of the electrode surface was increased (125.43 nm) because the surface became rougher, indicating modification of the electrode surface with the *SWCNTs-PPepx* nanocomposite. The prepared 3D network of nanocomposite layer was suitable for the immobilization of anti-CALR antibody because of the large surface area of the *SWCNTs-PPepx* nanocomposite layer. The unique structure of the *SWCNTs-PPepx* nanocomposite layer could provide a favorable microenvironment for the proteins to retain its good bioactivity. Figure 3C shows SEM and AFM images of the anti-CALR antibody-immobilized ITO surface. As clearly seen in this figure, the electrode surface morphology was changed, and the uniformity of the immobilized antibody distribution was observed. Therefore, a decline was seen in R_a (21.93 nm). The BSA blockage step created a variation in the morphological image of the ITO electrode surface and the BSA-immobilized surface looked like previous studies.[51] The R_a of the BSA-immobilized surface was 23.65 nm. Upon recognition of protein, changes in the morphological structure of the electrode surface occurred, which was the evidence of specific recognition between anti-CALR and CALR proteins. This specific immunointeraction increased the R_a, and it was found as 79.41 nm. These achieved results are in consonance with electrochemical analysis results.

3.4. Effects of the Polymer Layer Thickness, Anti-CALR Concentration, and Anti-CALR Incubation Times. The electrolyte solution used during the electropolymerization, scan numbers utilized for monomer electropolymerization, amount of anti-CALR antibody loaded on the ITO electrode surface, and incubation durations of anti-CALR and CALR molecules were optimized for the construction of CALR

https://doi.org/10.1021/acsbiomaterials.2c00499
ACS Biomater. Sci. Eng. 2022, 8, 3773−3784

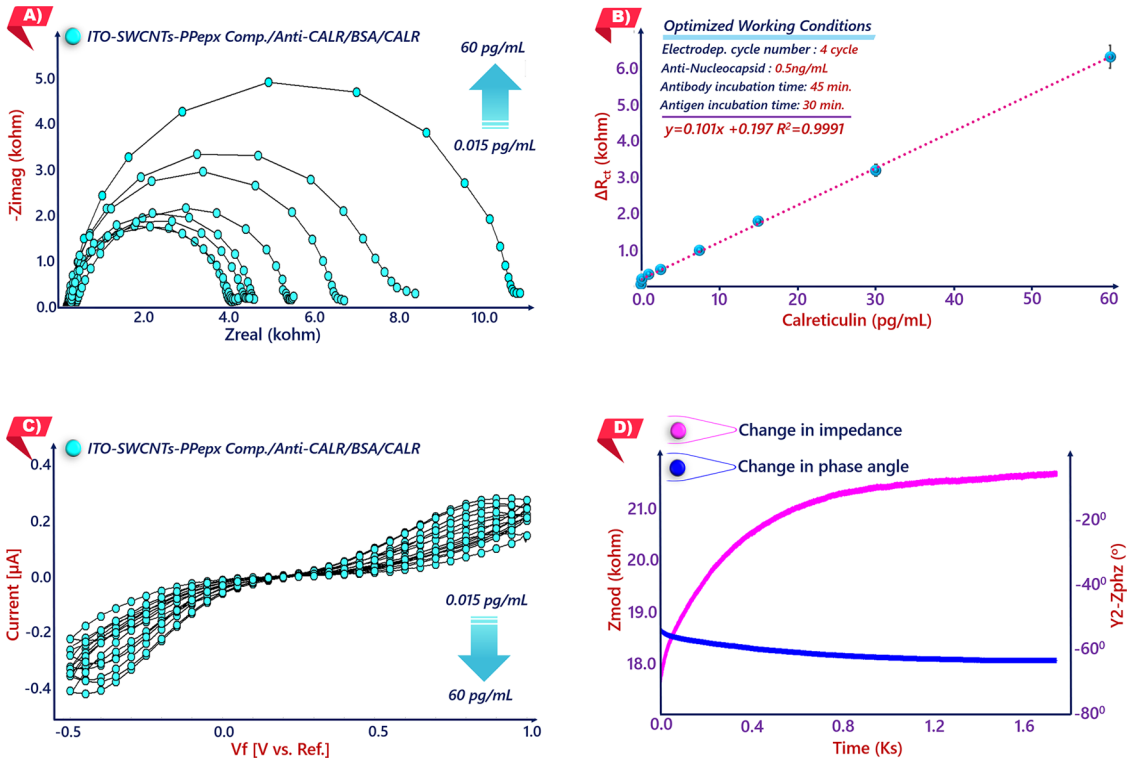

Figure 5. EIS (A) and CV (C) responses to different CALR concentrations, calibration curve for CALR analysis (B), and SFI response to CALR antigen (D).

biosensors. First of all, the electrolyte solution employed during the electropolymerization was investigated by using four different salts including TBAPCl, tetrabutylammonium tetrafluoroborate ($TBAPF_4$), tetrabutylammonium hexafluorophosphate ($TBAPF_6$), and lithium perchlorate-sodium perchlorate ($LiClO_4$-$NaClO_4$ 1:1). The calibration curves obtained with different electrolyte solutions are given in Figure SI-2. The maximum immunosensing signal was obtained, when TBAPCl was utilized as a supporting electrolyte. The effect of scan numbers of *Pepx* monomer electropolymerization was investigated by coating the monomer onto the ITO electrode with 2, 4, and 8 scan numbers. During the scan number optimization study, all the other parameters were constant. As shown in Figure 4A, it can be seen that the maximum impedimetric response of the immunosensor was obtained after four scan numbers. The immunosensor signal obtained after two scan numbers was low because sufficient active epoxy ends did not form on the ITO surface. The immunosensor developed with eight scan numbers had a low signal and this low signal might originate from thick polymer layer formation, which hindered electron transfer and caused high electron transfer resistance. Because of these reasons, four scan numbers were optimum for biosensor construction. Afterward, the effect of anti-CALR concentration on the immunosensor signal was investigated by incubating *SWCNTs-PPepx nanocomposite*-modified electrodes with different levels of anti-CALR (0.5 pg/mL; 2.5 pg/mL; 12.5 pg/mL) for 1 h. As observed in Figure 4B, the immunosensor had similar signals, and therefore, 0.5 pg/mL anti-CALR was utilized for biosensor development due to low fabrication cost. After optimization of the anti-CALR amount, the incubation time of anti-CALR was optimized. The nanocomposite-coated electrodes were incubated in anti-CALR antibody solution for 30, 45, and 60 min. After 30 min incubation, the biosensor had a low response toward CALR antigen owing to the insufficient amount of anti-CALR antibody molecule immobilization; 45-min incubation provided a good immunosensor signal, and thus, 45 min was the optimized duration for anti-CALR incubation (Figure 4C). Finally, the incubation duration of CALR was optimized. The ITO/*SWCNTs-PPepx nanocomposite*/anti-CALR/BSA electrodes were incubated in CALR solution for 30, 45, and 60 min. The responses of these immunosensors were similar, and therefore, 30 min was adequate time for CALR antigen incubation (Figure 4D).

3.5. Impedimetric Analysis of the Target Protein Calreticulin. The detection performance of the suggested electrochemical immunosensor was investigated utilizing the EIS technique. For this aim, eight different ITO/*SWCNTs-PPepx nanocomposite*/anti-CALR/BSA electrodes were incubated with increasing concentrations of CALR for 30 min. The differential charge transfer resistances were obtained against various levels of CALR antigen. Figure 5A shows the obtained impedimetric spectra after incubation with increasing amounts of CALR. The increase in the amount of CALR antigen caused an increase in the amount of immunocomplex and also, illustrated a gradual increment in R_{ct} values. In the same way, decreases were measured in CV peak currents with the increasing concentration of CALR (Figure 5C). The formed immunocomplex proteins caused formation of a protein barrier and prevented electron transport between the ITO surface and electrolyte solution. The proposed biosensor illustrated a wide linear range from 0.015 to 60 pg/mL (Figure 5B). The regression was found to be $\Delta R_{ct}[k\Omega] = 0.101[CALR] + 0.197$ with a correlation coefficient of 0.9991. The detection limit, quantification limit, and sensitivity were found as 4.6 fg/mL, 15.2 fg/mL, and 0.427 kΩ pg^{-1} mL cm^{-2}, respectively. The

https://doi.org/10.1021/acsbiomaterials.2c00499
ACS Biomater. Sci. Eng. 2022, 8, 3773−3784

Table 1. CALR Detection Methods (A) and CALR Concentration in Human Sera Samples Tested by the Developed Biosensor (B)

(A) biosensing system	detection method	detection range (pg/mL)	detection limit (pg/mL)	ref
ELISA	colorimetric	1300−200,000	1300	Raybiotech
ELISA	colorimetric	1300−200,000	1300	Thermofisher
ELISA	colorimetric	156−10,000	39	Mybiosource
ELISA	colorimetric	140.6−9000	140.6	Abcam
ELISA	colorimetric	160−10,000	100	Elabscience
SWCNTs-PPepx Comp. Modified Electrode	electrochemical	0.015−60	0.0046	present study

(B) sample	measured CALR level (pg/mL)	added CALR level (pg/mL)	measured CALR level (pg/mL)	SD and coefficient variation (%)[a]	recovery (%)	relative difference (%)
1	2.82	1.00	4.05	0.06−1.38	106.18	6.18
1	2.67	1.00	3.97		108.30	8.30
1	2.82	30.00	32.96	0.14−0.42	100.45	0.45
1	2.67	30.00	32.77		100.30	0.30
2	2.83	1.00	3.89	0.23−5.64	101.54	1.54
2	3.06	1.00	4.22		103.87	3.87
2	2.83	30.00	32.68	0.83−2.59	99.52	−0.48
2	3.06	30.00	31.50		95.28	−4.72
3	5.33	1.00	6.38	0.06−0.87	100.93	0.93
3	5.24	1.00	6.31		101.11	1.11
3	5.33	30.00	35.93	0.68−1.87	101.72	1.72
3	5.24	30.00	36.89		104.70	4.70
4	5.83	1.00	7.09	0.12−1.64	103.88	3.88
4	6.04	1.00	7.26		103.07	3.07
4	5.83	30.00	35.90	0.83−2.26	100.22	0.22
4	6.04	30.00	37.07		102.85	2.85
5	2.33	1.00	3.47	0.02−0.60	104.13	4.13
5	2.42	1.00	3.50		102.30	2.30
5	2.33	30.00	33.18	0.31−0.93	102.61	2.61
5	2.42	30.00	32.75		101.00	1.00

[a]SD, standard deviation.

detection limit, linear range, and sensitivity of the proposed biosensor were compared to other detection methods of CALR (Table 1A). These results indicated that the constructed immunosensor had suitable performance for CALR detection in the low femtogram level which was not possible with ELISA. The *SWCNTs-PPepx* nanocomposite matrix provided high electrical conductivity due to *SWCNTs* and *PPepx*-conjugated polymer for electron transfer reactions and high stability. Thus, this layer supported the electrochemical signal and provided a low detection limit for the proposed biosensor. The electrodeposition of *SWCNTs* incorporating polymerization of the *Pepx* monomer onto disposable ITO electrodes offered the easy control of the thickness of the nanocomposite layer and electrode surfaces homologous to each other were obtained. More repeatable and reproducible results were obtained with the use of these electrodes, and the obtained repeatability and reproducibility results were supported by statistical analysis methods including the *F*-Test and *T*-Test.

SFI analysis is the most appropriate technique to follow the kinetic biointeraction between antibody and its target antigen. During this experiment, impedance is recorded at single frequency, which was determined with the help of the Bode plot.[52] In this study, a target CALR antigen solution (phosphate buffer, pH 7.4) was prepared and used for SFI analysis. The ITO/*SWCNTs-PPepx nanocomposite*/anti-CALR/BSA electrode immersed in this solution at the three-electrode system and the time-dependent variations at the single impedance were recorded. As observed in Figure 5D, an increase in impedance (pink plot) was seen and this increment demonstrated the successful interaction.

The repeatability of the sensing system was evaluated by recording the R_{ct} responses of 30 ITO/*SWCNTs-PPepx nanocomposite*/anti-CALR/BSA electrodes after incubation in PBS solution containing CALR antigen with three different concentrations. To analyze the repeatability performance of the biosensor, Grubbs' and Dixons' tests were performed. Grubbs' test is employed to determine a single outlier in a normally data test.[53,54] In this test, the results attained after Grubbs' test application were compared to the fixed value (level of significance) present in Grubbs' table. The low and high Grubbs' test values were calculated as 1.476 (for 0.1 pg/mL); 1.27 (for 15 pg/mL); 0.80 (for 20 pg/mL) and 1.492 (for 0.1 pg/mL); 2.025 (for 15 pg/mL); 2.195 (for 30 pg/mL), respectively. The calculated values were lower than Grubbs' critical tabulated value (2.29, α = 0.05). Apart from Grubbs' test, the Dixon test was also utilized for the testing outlier. The low and high Dixon test values were calculated as 0.0 (for 0.1 pg/mL); 0.115 (for 15 pg/mL); 0.0 (for 30 pg/mL) and 0.143 (for 0.1 pg/mL); 0.403 (for 15 pg/mL); 0.371 (for 30 pg/mL), respectively. The calculated values were lower than Dixon's critical tabulated value (0.477), and therefore, according to Grubbs' and Dixons' statistical evaluation rule, the data sets have no outliers.

The reproducibility of the study was investigated by measuring the impedimetric responses of 60 bioelectrodes after incubation in PBS solution containing CALR antigen with three different concentrations. The reproducibility study was

https://doi.org/10.1021/acsbiomaterials.2c00499
ACS Biomater. Sci. Eng. 2022, 8, 3773−3784

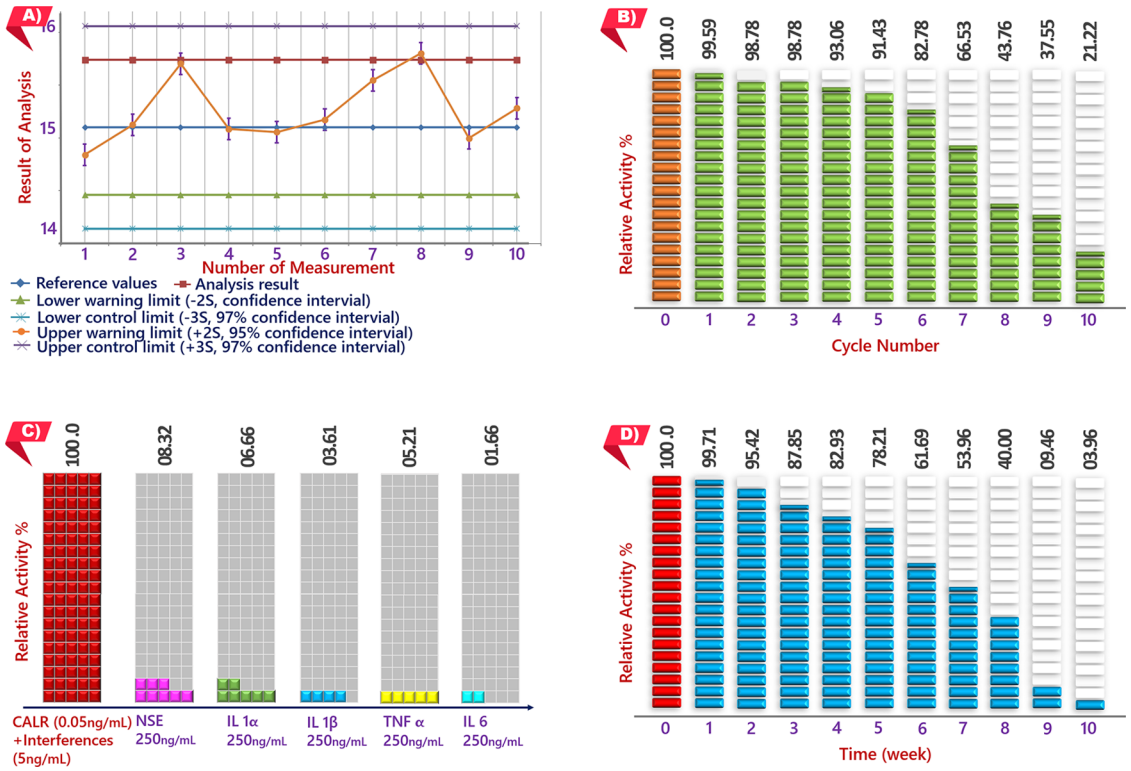

Figure 6. Quality control chart (A), reusability (B), selectivity (C), and storage stability (D) of the proposed biosensor.

also performed with two researchers by measuring three different CALR concentrations (0.1, 15, and 30 pg/mL) for 10 times under the same conditions in different days. The obtained results were evaluated with the Horwitz test; the Horwitz ratio displayed the acceptability of analysis techniques, and this ratio was calculated by using relative standard deviation (RSD, %) and predicted relative standard deviation determined by using the Horwitz equation.[55] As a result of this statistical test, Horwitz ratios of the 15 pg/mL data set were found as 0.72 and 0.56. These values were lower than 2, and they proved the excellent training and experience.

To evaluate the reproducibility test results (for 15 pg/mL), the *T*-test and *F*-test were carried out to check the means and the distribution of the groups, respectively. A two-sample *T*-test assuming equal variances was used to find the statistical significance.[56] The calculated *T*-amount was lower than the *T*-critical two-tail amount ($0.69 < 2.10$), and thus, the averages of data were not importantly distinct from each other and the attained value was not statistically significant. The calculated *F*-value was lower than the *F*-critical tabulated value ($1.679 < 4.026$). The obtained result illustrated that the distribution of the data set was not significantly different from each other. The pooled standard deviation was found as 0.369, and low RSD proved good reproducibility and acceptable precision. Figure 6A illustrates the quality control chart of the system, and this chart illustrated the variations during the measurements. The reference value of this chart was 15 pg/mL. Upper and lower warning limits were calculated as 15.64 and 14.36 pg/mL, respectively. Upper and lower control limits were calculated as 15.96 and 14.04 pg/mL, respectively. As seen in Figure 6A, the measurement results were present in these limits, and the results were acceptable for analysis. Consequently, the obtained RSD values confirmed an acceptable repeatability and reproducibility of the biosensor development procedure and electrochemical analyses.

To test the reusability of the prepared electrode, regeneration ability of the biosensor was studied. After each detection of CALR protein, the utilized electrode was regenerated by incubation in HCl solution (0.01 M) for 5 min, and after that, it was washed with ultrapure water. The regeneration process continued until the electrode failed. The biosensor retained 82.78% its initial signal after six regeneration cycles. This result indicated good reusability performance of the biosensor (Figure 6B). To investigate the selectivity suggested immunosensor, some biomarkers such as NSE, TNF-α, IL6, IL-1α, and IL-1β with higher concentration (250 pg/mL) than CALR (2.5 pg/mL) were utilized, and the impedimetric signal toward these antigens was tested with the suggested immunosensor. As observed in Figure 6C, the suggested biosensor gave insignificant responses to these biomarkers at high concentration levels. The obtained results illustrated the specific binding of anti-CALR to CALR and the selectivity of this biosensor. For investigation of the storage stability of the suggested biosensor, 10 different electrodes fabricated under the same conditions were used to check their responses against 45 pg/mL CALR. The prepared bioelectrodes were stored at 4 °C, and each week, the electrochemical response of the related electrode was recorded. The proposed immunosensor retained 61.69% of its initial signal after 6 weeks. The obtained good storage stability was attributed to successful nanocomposite layer coating on the ITO electrode, which supported the immobilization of anti-calreticulin (Figure 6D).

3.6. Analytical Applicability of the Biosensor for CALR Analysis in Human Sera. The clinical applicability of the suggested immunosensor was appraised by measurement of CALR in human serum. First of all, before analysis, human sera

https://doi.org/10.1021/acsbiomaterials.2c00499
ACS Biomater. Sci. Eng. 2022, 8, 3773−3784

samples were diluted 1000 times with phosphate buffer. The CALR level of diluted serum samples was analyzed with the suggested biosensor. After that, the serum samples were spiked with two different levels (1 and 30 pg/mL) of CALR protein to test the accuracy of the sensing system. After adding CALR protein, these serum samples were analyzed with the proposed biosensor. EIS measurements were performed in duplicate, and recovery results of the suggested biosensing technique changed from 95.28 to 108.30% which confirmed that the proposed biosensor was feasible for the analysis of CALR at low levels in human sera.

4. CONCLUSIONS

In summary, a novel hybrid nanocomposite material *SWCNTs-PPepx* was covered onto a low-cost and disposable ITO platform in order to fabricate an ultrasensitive and selective immunosensor for CALR analysis in human sera. The utilized biosensor fabrication strategy provided a conductive immobilization matrix with a large surface area. The use of the *SWCNTs-PPepx* nanocomposite not only facilitated the electron transfer between the electrolyte and working electrode surface, but also it provided attachment points for anti-CALR biorecognition molecules. The changes in R_{ct} were linearly dependent on the CALR level in the linear range of 0.015−60 pg/mL with a correlation coefficient of 0.9991. The proposed biosensor had good selectivity, robust storage stability, and simple applicability. Furthermore, according to statistical analysis techniques, the proposed system was a reliable and successful tool for CALR analysis. Finally, the suggested tool was further applied for the analysis of CALR concentration in human sera with satisfactory results. In conclusion, the described procedure could also be used for the detection and quantification of the other protein biomarker in the fields of clinical diagnosis.

■ ASSOCIATED CONTENT

Supporting Information

The Supporting Information is available free of charge at https://pubs.acs.org/doi/10.1021/acsbiomaterials.2c00499.

Materials and reagents used during the biosensor development (PDF)

■ AUTHOR INFORMATION

Corresponding Author

Elif Burcu Aydın − *Scientific and Technological Research Center, Tekirdağ Namık Kemal University, Tekirdağ 59030, Turkey;* orcid.org/0000-0002-1982-4128; Email: ebbahadir@nku.edu.tr

Authors

Muhammet Aydın − *Scientific and Technological Research Center, Tekirdağ Namık Kemal University, Tekirdağ 59030, Turkey*

Mustafa Kemal Sezgintürk − *Faculty of Engineering, Bioengineering Department, Çanakkale Onsekiz Mart University, Çanakkale 17100, Turkey;* orcid.org/0000-0003-3042-1087

Complete contact information is available at: https://pubs.acs.org/10.1021/acsbiomaterials.2c00499

Notes

The authors declare no competing financial interest.

■ ACKNOWLEDGMENTS

The authors gratefully acknowledge support from project FHD-2021-3533 of the Scientific and Technological Research Council of Çanakkale Onsekiz Mart University. We thank Assoc. Prof. Pınar Ilgın for her support in the FTIR analysis.

■ REFERENCES

(1) Ou, D.; Sun, D.; Lin, X.; Liang, Z.; Zhong, Y.; Chen, Z. A dual-aptamer-based biosensor for specific detection of breast cancer biomarker HER2 via flower-like nanozymes and DNA nanostructures. *J. Mater. Chem. B* **2019**, *7*, 3661−3669.

(2) Ammar, M. B.; Ayachi, F. L.; Ksantini, R.; Mahjoubi, H. Data warehouse for machine learning: application to breast cancer diagnosis. *Procedia Comput. Sci.* **2022**, *196*, 692−698.

(3) Kang, U.-B.; Ahn, Y.; Lee, J. W.; Kim, Y.-H.; Kim, J.; Yu, M.-H.; Noh, D.-Y.; Lee, C. Differential profiling of breast cancer plasma proteome by isotope-coded affinity tagging method reveals biotinidase as a breast cancer biomarker. *BMC Cancer* **2010**, *10*, 114.

(4) Campuzano, S.; Pedrero, M.; Pingarrón, J. M. Non-invasive breast cancer diagnosis through electrochemical biosensing at different molecular levels. *Sensors* **2017**, *17*, 1993.

(5) Pereira, A.; Sales, M.; Rodrigues, L., Biosensors for rapid detection of breast cancer biomarkers. In *Advanced Biosensors for Health Care Applications*; Elsevier: 2019; 71−103.

(6) Wang, X.-Y.; Feng, Y.-G.; Wang, A.-J.; Mei, L.-P.; Yuan, P.-X.; Luo, X.; Feng, J.-J. A facile ratiometric electrochemical strategy for ultrasensitive monitoring HER2 using polydopamine-grafted-ferrocene/reduced graphene oxide, Au@ Ag nanoshuttles and hollow Ni@ PtNi yolk-shell nanocages. *Sens. Actuators B Chem.* **2021**, *331*, No. 129460.

(7) Lwin, Z.-M.; Guo, C.; Salim, A.; Yip, G. W.-C.; Chew, F.-T.; Nan, J.; Thike, A. A.; Tan, P.-H.; Bay, B.-H. Clinicopathological significance of calreticulin in breast invasive ductal carcinoma. *Mod. Pathol.* **2010**, *23*, 1559−1566.

(8) Zamanian, M.; Hamadneh, L. A. Q.; Veerakumarasivam, A.; Rahman, S. A.; Shohaimi, S.; Rosli, R. Calreticulin mediates an invasive breast cancer phenotype through the transcriptional dysregulation of p53 and MAPK pathways. *Cancer Cell Int.* **2016**, *16*, 56.

(9) Ramesh, B. S.; Giorgakis, E.; Lopez-Davila, V.; Dashtarzheneha, A. K.; Loizidou, M. Detection of cell surface calreticulin as a potential cancer biomarker using near-infrared emitting gold nanoclusters. *Nanotechnology* **2016**, *27*, No. 285101.

(10) Miao, S.; Ge, Y.; Yi, Z.; Feng, Q. Screening of Aptamer for Breast Cancer Biomarker Calreticulin and Its Application to Detection of Serum and Recognition of Breast Cancer Cell. *Chin. J. Anal. Chem.* **2020**, *48*, 642−649.

(11) Lee, H.-H.; Lim, C.-A.; Cheong, Y.-T.; Singh, M.; Gam, L.-H. Comparison of protein expression profiles of different stages of lymph nodes metastasis in breast cancer. *Int. J. Biol. Sci.* **2012**, *8*, 353.

(12) Cruz-Ramos, E.; Sandoval-Hernandez, A.; Tecalco-Cruz, A. C. Differential expression and molecular interactions of chromosome region maintenance 1 and calreticulin exportins in breast cancer cells. *J. Steroid Biochem. Mol. Biol.* **2019**, *185*, 7−16.

(13) Ni, M.; Wei, W.; Wang, Y.; Zhang, N.; Ding, H.; Shen, C.; Zheng, F. Serum levels of calreticulin in correlation with disease activity in patients with rheumatoid arthritis. *J. Clin. Immunol.* **2013**, *33*, 947−953.

(14) Jeong, S.; Park, M.-J.; Song, W.; Kim, H.-S. Current immunoassay methods and their applications to clinically used biomarkers of breast cancer. *Clin. Biochem.* **2020**, *78*, 43−57.

(15) Aydın, M.; Aydın, E. B.; Sezgintürk, M. K. Electrochemical immunosensor for CDH22 biomarker based on benzaldehyde substituted poly (phosphazene) modified disposable ITO electrode: A new fabrication strategy for biosensors. *Biosens. Bioelectron.* **2019**, *126*, 230−239.

(16) Mittal, S.; Kaur, H.; Gautam, N.; Mantha, A. K. Biosensors for breast cancer diagnosis: A review of bioreceptors, biotransducers and signal amplification strategies. *Biosens. Bioelectron.* **2017**, *88*, 217−231.
(17) Zhou, C.; Liu, D.; Xu, L.; Li, Q.; Song, J.; Xu, S.; Xing, R.; Song, H. A sensitive label−free amperometric immunosensor for alpha-fetoprotein based on gold nanorods with different aspect ratio. *Sci. Rep.* **2015**, *5*, 9939.
(18) Diaconu, I.; Cristea, C.; Hârceagă, V.; Marrazza, G.; Berindan-Neagoe, I.; Săndulescu, R. Electrochemical immunosensors in breast and ovarian cancer. *Clin. Chim. Acta* **2013**, *425*, 128−138.
(19) Arya, S. K.; Estrela, P. Recent advances in enhancement strategies for electrochemical ELISA-based immunoassays for cancer biomarker detection. *Sensors* **2018**, *18*, 2010.
(20) Khanmohammadi, A.; Aghaie, A.; Vahedi, E.; Qazvini, A.; Ghanei, M.; Afkhami, A.; Hajian, A.; Bagheri, H. Electrochemical biosensors for the detection of lung cancer biomarkers: A review. *Talanta* **2020**, *206*, No. 120251.
(21) Hassanpour, S.; Hasanzadeh, M. Label-free electrochemical-immunoassay of cancer biomarkers: Recent progress and challenges in the efficient diagnosis of cancer employing electroanalysis based on point of care (POC). *Microchem. J.* **2021**, *168*, No. 106424.
(22) Jayanthi, V. S. A.; Das, A. B.; Saxena, U. Fabrication of an immunosensor for quantitative detection of breast cancer biomarker UBE2C. *RSC Adv.* **2019**, *9*, 16738−16745.
(23) Aydın, E. B.; Aydın, M.; Sezgintürk, M. K. A highly sensitive immunosensor based on ITO thin films covered by a new semi-conductive conjugated polymer for the determination of TNFα in human saliva and serum samples. *Biosens. Bioelectron.* **2017**, *97*, 169−176.
(24) Feng, Y.-G.; Zhu, J.-H.; Wang, A.-J.; Mei, L.-P.; Luo, X.; Feng, J.-J. AuPt nanocrystals/polydopamine supported on open-pored hollow carbon nanospheres for a dual-signaling electrochemical ratiometric immunosensor towards h-FABP detection. *Sens. Actuators B Chem.* **2021**, *346*, No. 130501.
(25) Chikkaveeraiah, B. V.; Bhirde, A. A.; Morgan, N. Y.; Eden, H. S.; Chen, X. Electrochemical immunosensors for detection of cancer protein biomarkers. *ACS Nano* **2012**, *6*, 6546−6561.
(26) Lim, S. A.; Ahmed, M. U. Electrochemical immunosensors and their recent nanomaterial-based signal amplification strategies: A review. *RSC Adv.* **2016**, *6*, 24995−25014.
(27) Zhang, Y.; Zhang, R.; Yang, X.; Qi, H.; Zhang, C. Recent advances in electrogenerated chemiluminescence biosensing methods for pharmaceuticals. *J. Pharm. Anal.* **2019**, *9*, 9−19.
(28) Védrine, C.; Fabiano, S.; Tran-Minh, C. Amperometric tyrosinase based biosensor using an electrogenerated polythiophene film as an entrapment support. *Talanta* **2003**, *59*, 535−544.
(29) Ding, S.-J.; Chang, B.-W.; Wu, C.-C.; Lai, M.-F.; Chang, H.-C. Impedance spectral studies of self-assembly of alkanethiols with different chain lengths using different immobilization strategies on Au electrodes. *Anal. Chim. Acta* **2005**, *554*, 43−51.
(30) Ohno, R.; Ohnuki, H.; Wang, H.; Yokoyama, T.; Endo, H.; Tsuya, D.; Izumi, M. Electrochemical impedance spectroscopy biosensor with interdigitated electrode for detection of human immunoglobulin A. *Biosens. Bioelectron.* **2013**, *40*, 422−426.
(31) Aydın, E. B.; Aydın, M.; Sezgintürk, M. K. Highly selective and sensitive sandwich immunosensor platform modified with MUA-capped GNPs for detection of spike Receptor Binding Domain protein: a precious marker of COVID 19 infection. *Sens. Actuators B Chem.* **2021**, *345*, No. 130355.
(32) Aydın, E. B.; Aydın, M.; Sezgintürk, M. K. New Impedimetric Sandwich Immunosensor for Ultrasensitive and Highly Specific Detection of Spike Receptor Binding Domain Protein of SARS-CoV-2. *ACS Biomater. Sci. Eng.* **2021**, *7*, 3874−3885.
(33) Sandhyarani, N., Surface modification methods for electrochemical biosensors. In *Electrochemical Biosensors*; Elsevier: 2019; 45−75.
(34) Maduraiveeran, G.; Sasidharan, M.; Ganesan, V. Electrochemical sensor and biosensor platforms based on advanced nanomaterials for biological and biomedical applications. *Biosens. Bioelectron.* **2018**, *103*, 113−129.
(35) Govindhan, M.; Adhikari, B.-R.; Chen, A. Nanomaterials-based electrochemical detection of chemical contaminants. *RSC Adv.* **2014**, *4*, 63741−63760.
(36) Chen, Y.; Yuan, P.-X.; Wang, A.-J.; Luo, X.; Xue, Y.; Zhang, L.; Feng, J.-J. A novel electrochemical immunosensor for highly sensitive detection of prostate-specific antigen using 3D open-structured PtCu nanoframes for signal amplification. *Biosens. Bioelectron.* **2019**, *126*, 187−192.
(37) Gao, C.; Guo, Z.; Liu, J.-H.; Huang, X.-J. The new age of carbon nanotubes: an updated review of functionalized carbon nanotubes in electrochemical sensors. *Nanoscale* **2012**, *4*, 1948−1963.
(38) Dhand, C.; Solanki, P. R.; Datta, M.; Malhotra, B. D. Polyaniline/Single-walled carbon nanotubes composite based triglyceride biosensor. *Electroanalysis* **2010**, *22*, 2683−2693.
(39) Zamani, F. G.; Moulahoum, H.; Ak, M.; Demirkol, D. O.; Timur, S. Current trends in the development of conducting polymers-based biosensors. *TrAC, Trends Anal. Chem.* **2019**, *118*, 264−276.
(40) Teles, F. R. R.; Fonseca, L. P. Applications of polymers for biomolecule immobilization in electrochemical biosensors. *Mater. Sci. Eng. C* **2008**, *28*, 1530−1543.
(41) Ahuja, T.; Kumar, D. Recent progress in the development of nano-structured conducting polymers/nanocomposites for sensor applications. *Sens. Actuators B Chem.* **2009**, *136*, 275−286.
(42) Aydın, E. B.; Aydın, M.; Sezgintürk, M. K. The development of an ultra-sensitive electrochemical immunosensor using a PPyr-NHS functionalized disposable ITO sheet for the detection of interleukin 6 in real human serums. *New J. Chem.* **2020**, *44*, 14228−14238.
(43) Shafaat, A.; Faridbod, F.; Ganjali, M. R. Label-free detection of cytochrome C by a conducting polymer-based impedimetric screen-printed aptasensor. *New J. Chem.* **2018**, *42*, 6034−6039.
(44) Aydın, E. B.; Aydın, M.; Sezgintürk, M. K. Ultrasensitive and Selective Impedimetric Determination of Prostate Specific Membrane Antigen Based on Di-Succinimide Functionalized Polythiophene Covered Cost-Effective Indium Tin Oxide. *Macromol. Biosci.* **2021**, *21*, No. 2100173.
(45) Aydın, E. B.; Aydın, M.; Sezgintürk, M. K. Highly sensitive electrochemical immunosensor based on polythiophene polymer with densely populated carboxyl groups as immobilization matrix for detection of interleukin 1β in human serum and saliva. *Sens. Actuators B Chem.* **2018**, *270*, 18−27.
(46) Aydın, E. B.; Aydın, M.; Sezgintürk, M. K. Selective and ultrasensitive electrochemical immunosensing of NSE cancer biomarker in human serum using epoxy-substituted poly (pyrrole) polymer modified disposable ITO electrode. *Sens. Actuators B Chem.* **2020**, *306*, No. 127613.
(47) Maeda, S.; Corradi, R.; Armes, S. P. Synthesis and characterization of carboxylic acid-functionalized polypyrrole-silica microparticles. *Macromolecules* **1995**, *28*, 2905−2911.
(48) Khan, W.; Kapoor, M.; Kumar, N. Covalent attachment of proteins to functionalized polypyrrole-coated metallic surfaces for improved biocompatibility. *Acta Biomater.* **2007**, *3*, 541−549.
(49) Liu, Y.; Zhu, Y.; Zeng, Y.; Xu, F. An effective amperometric biosensor based on gold nanoelectrode arrays. *Nanoscale Res. Lett.* **2009**, *4*, 210−215.
(50) Simão, E. P.; Silva, D. B.; Cordeiro, M. T.; Gil, L. H.; Andrade, C. A.; Oliveira, M. D. Nanostructured impedimetric lectin-based biosensor for arboviruses detection. *Talanta* **2020**, *208*, No. 120338.
(51) Aydın, E. B.; Aydın, M.; Sezgintürk, M. K. Fabrication of electrochemical immunosensor based on acid-substituted poly (pyrrole) polymer modified disposable ITO electrode for sensitive detection of CCR4 cancer biomarker in human serum. *Talanta* **2021**, *222*, No. 121487.
(52) Aydın, E. B.; Aydın, M.; Sezgintürk, M. K. Electrochemical immunosensor based on chitosan/conductive carbon black composite modified disposable ITO electrode: An analytical platform for p53 detection. *Biosens. Bioelectron.* **2018**, *121*, 80−89.

https://doi.org/10.1021/acsbiomaterials.2c00499
ACS Biomater. Sci. Eng. 2022, 8, 3773−3784

(53) Jain, R. B. A recursive version of Grubbs' test for detecting multiple outliers in environmental and chemical data. *Clin. Biochem.* **2010**, *43*, 1030−1033.
(54) Barbato, G.; Barini, E. M.; Genta, G.; Levi, R. Features and performance of some outlier detection methods. *J. Appl. Stat.* **2011**, *38*, 2133−2149.
(55) Horwitz, W.; Albert, R. The Horwitz ratio (HorRat): a useful index of method performance with respect to precision. *J. AOAC Int.* **2006**, *89*, 1095−1109.
(56) Peng, L.; Tong, T. A note on a two-sample T test with one variance unknown. *Stat. Methodol.* **2011**, *8*, 528−534.

https://doi.org/10.1021/acsbiomaterials.2c00499
ACS Biomater. Sci. Eng. 2022, 8, 3773−3784